Subnanometre platinum clusters as highly active and selective catalysts for the oxidative dehydrogenation of propane

Stefan Vajda[1,2,3]*, Michael J. Pellin[4], Jeffrey P. Greeley[2], Christopher L. Marshall[1], Larry A. Curtiss[1,2,4]*, Gregory A. Ballentine[1†], Jeffrey W. Elam[5], Stephanie Catillon-Mucherie[1], Paul C. Redfern[1], Faisal Mehmood[4] and Peter Zapol[1,2,4]

Small clusters are known to possess reactivity not observed in their bulk analogues, which can make them attractive for catalysis[1-6]. Their distinct catalytic properties are often hypothesized to result from the large fraction of under-coordinated surface atoms[7-9]. Here, we show that size-preselected Pt$_{8-10}$ clusters stabilized on high-surface-area supports are 40–100 times more active for the oxidative dehydrogenation of propane than previously studied platinum and vanadia catalysts, while at the same time maintaining high selectivity towards formation of propylene over by-products. Quantum chemical calculations indicate that under-coordination of the Pt atoms in the clusters is responsible for the surprisingly high reactivity compared with extended surfaces. We anticipate that these results will form the basis for development of a new class of catalysts by providing a route to bond-specific chemistry, ranging from energy-efficient and environmentally friendly synthesis strategies to the replacement of petrochemical feedstocks by abundant small alkanes[10,11].

The oxidative dehydrogenation (ODH) of alkanes is a reaction that is exothermic overall and is, thus, an attractive alternative to dehydrogenation of alkanes, which is an endothermic process requiring significant energy input. However, current ODH catalysts have limited activity and/or poor selectivity resulting from an inability to prevent complete oxidation[12]. The reaction scheme for propane ODH is shown in formula (1) and includes other competing pathways that lead to CO_x species.
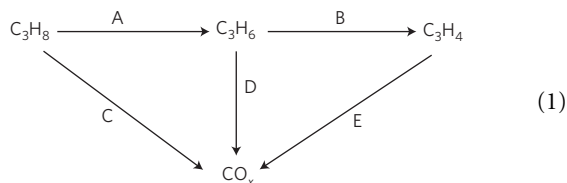
In formula (1), channel A corresponds to the pathway for propylene production and channels B, C, D and E result in less desirable products.
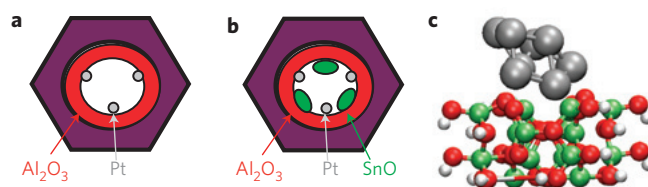

Figure 1 | Depiction of the catalytic system. **a,b**, Illustration of Pt clusters deposited in AAO membrane with ALD coating of Al_2O_3 (**a**), and with added SnO (**b**). **c**, Structure of Pt$_8$ cluster on an Al_2O_3 surface from density functional calculations. In this structure there are four Pt–O distances between 2.2 and 2.4 Å and the closest Pt–Al distance is 2.55 Å. See Supplementary Information for more details.

Methods for producing size-selected clusters and soft-landing them on catalytic supports are now well established[13–16]. However, testing these catalytic clusters under realistic reaction conditions requires supports on which the clusters resist sintering. Both alumina and tin oxide surfaces are known to stabilize platinum clusters[15,17]. We used atomic layer deposition (ALD) to coat porous anodized aluminium oxide (AAO, Anopore) membranes with alumina (Al_2O_3/AAO) before Pt-cluster deposition as illustrated in Fig. 1. The ALD process ensures a uniform surface chemistry[18] for the attachment of the clusters. Membranes were used in this investigation because they provide a high surface area so that high dispersions of size-selected clusters can be achieved, and catalytic tests under well-defined conditions can be carried out. The Pt$_{8-10}$ clusters were mass-selected, and a total of 900 ($\pm$135) ng Pt was soft-landed on the large pore side ($\sim$200 nm diameter) of the membrane. A pair of membranes with identical Pt$_{8-10}$ and alumina loadings were synthesized; one was left as-is and one was treated with an equivalent of two-monolayer-thick tin oxide ALD, resulting in an overcoat of the alumina support around the platinum clusters with tin oxide (SnO/Al_2O_3/AAO, Fig. 1).

Synchrotron grazing-incidence small-angle X-ray scattering studies of alumina-supported size-selected Pt clusters carried out in our laboratory[15] have provided evidence for the stability and

[1]Chemical Sciences and Engineering Division, Argonne National Laboratory, 9700 South Cass Avenue, Argonne, Illinois 60439, USA, [2]Center for Nanoscale Materials, Argonne National Laboratory, 9700 South Cass Avenue, Argonne, Illinois 60439, USA, [3]Department of Chemical Engineering, School of Engineering & Applied Science, Yale University, 9 Hillhouse Avenue, New Haven, Connecticut 06520, USA, [4]Materials Science Division, Argonne National Laboratory, 9700 South Cass Avenue, Argonne, Illinois 60439, USA, [5]Energy Systems Division, Argonne National Laboratory, 9700 South Cass Avenue, Argonne, Illinois 60439, USA. †Present Address: Max-Planck-Institut für Metallforschung, Stuttgart, Germany. *e-mail: vajda@anl.gov; curtiss@anl.gov.
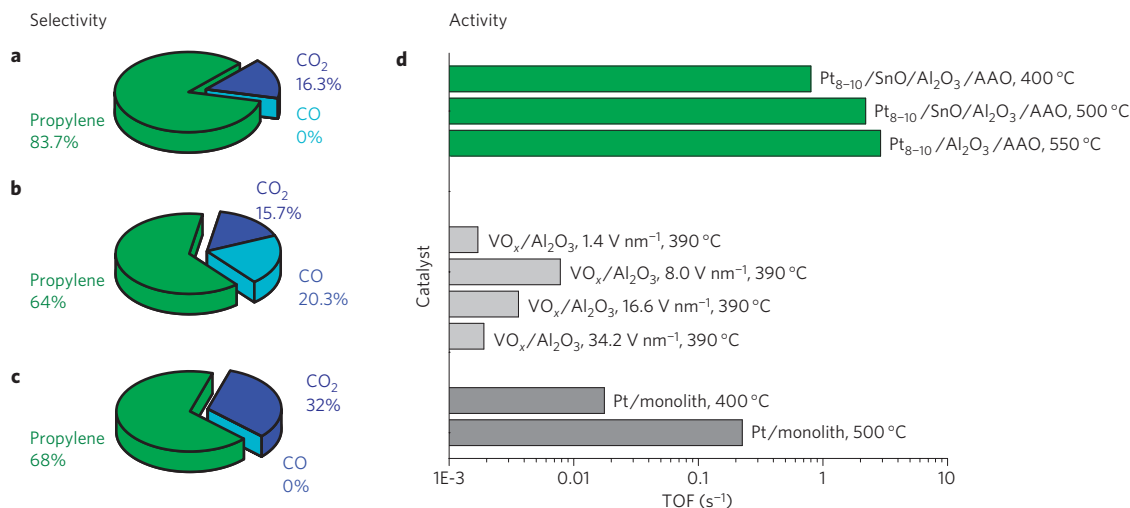
1

Figure 2 | Catalyst activity and selectivity. a–c, Selectivity of the Pt_{8-10}-based catalysts at various temperatures and support compositions: SnO/Al_2O_3 at 400 °C (**a**), SnO/Al_2O_3 at 500 °C (**b**) and Al_2O_3 at 550 °C (**c**). **d**, TOFs of propylene produced on the Pt_{8-10} catalysts (green) and reference ODH catalysts (grey) expressed as number of propylene molecules formed per metal atom. Pt monolith and vanadia data from refs 29 and 22, respectively. See Supplementary Information for more details.
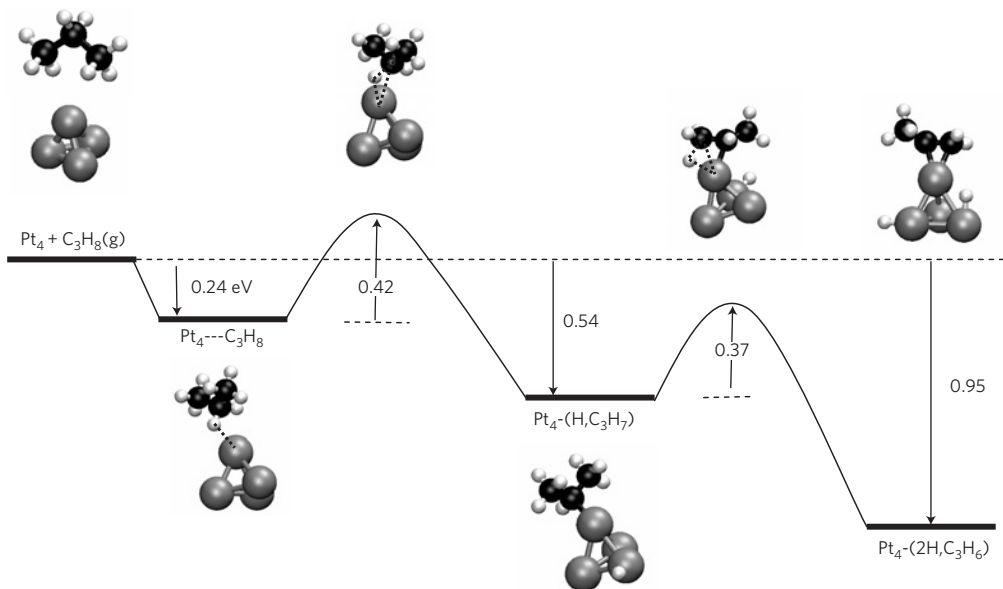

Figure 3 | Reaction path. Diagram of primary reaction steps in channel A (see formula (1)) from DFT calculations for the dehydrogenation of propane on a Pt_4 cluster leading to formation of propylene adsorbed on the cluster. Energies (in eV) of the equilibrium structures are relative to the reactants. Energy barriers for the transition state structures are relative to the preceding equilibrium structure ('true' barriers). The first barrier corresponds to breaking of the first C–H bond (on the CH_2 group) and the second barrier corresponds to breaking of the second C–H bond (on a CH_3 group). A number of other reaction steps involving hydrogen migration are not included in this diagram. The dotted lines in the structures indicate partial bonds. See Supplementary Information for more details of structures and energies and other reaction pathways.

shape of the Pt clusters. The supported clusters, similar to those used in this study, showed no evidence of agglomeration over a temperature range of 20–400 °C, and they maintained a three-dimensional structure. At the higher temperatures used in the catalytic testing in this study, there was also no evidence of any change in cluster size, as there was no change in selectivity or activity after 30 h of testing. We have also carried out density functional theory (DFT) calculations[14] to investigate the structure of a Pt_8 cluster on a θ-alumina surface. The structure (Fig. 1) indicates that the cluster maintains its three-dimensional structure, as is found in the X-ray studies. The Pt cluster forms Pt–O bonds with the surface, resulting in significant charge transfer to the cluster. The binding of the cluster to the surface (~3 eV) is consistent with the stability of the subnanometre Pt_8 clusters on alumina, but does not significantly affect the cluster's chemical reactivity (see

below). In addition, we carried out calculations to investigate the stability of a positively charged Pt_8 cluster on alumina and found that it withdraws electrons from the surface and becomes negatively charged as in the case of the supported neutral cluster (see below). In a sense, these highly uniform clusters can be considered an ideal model of a single-site catalyst on technologically relevant supports, in which all active sites closely resemble each other[2,19,20].

The catalyst tests were carried out under atmospheric pressure in a flow reactor at temperatures from 400 to 550 °C by using 10 s.c.c.m. total flow of reactants in argon carrier gas with 2.63 and 2.73 mol% of oxygen and propane, respectively. The temperature range was chosen to give a direct comparison with the performance of reported Pt-and VO_x-based ODH catalysts. The measured turnover frequencies (TOFs) are shown in Fig. 2, along with the highest reported values for platinum and vanadia. The TOFs were

calculated as the number of propylene molecules produced per Pt atom per second (see Supplementary Information for details of the method of calculation). The activity and selectivity at $500\,^{\circ}$C was unchanged over 30 h of testing.

The main finding of this study is that the activity of the Pt_{8-10} catalyst is markedly higher than any reported platinum or vanadia-based ODH catalysts. In fact, at $400\,^{\circ}$C, the observed TOFs are 40–100 times higher than those previously reported. The product distribution (Fig. 2) indicates that selectivity for propylene over the formation of carbon oxide species is also achieved. The total conversion approaches $25\% \pm 4\%$ at high temperatures. The uncertainty in the reported TOF is around 15%, determined primarily by the uncertainty in the amount of Pt loading. The uncertainty in conversion rates is given by the precision at determining the diameter of the Pt spots on the membrane using grazing-incidence small-angle X-ray scattering on poreless flat-alumina supported Pt clusters prepared under identical deposition conditions.

To understand the observed high activity of small Pt clusters for propane ODH, we carried out DFT calculations on key steps for channel A in the reaction diagram in formula (1). Channel A is the predominant channel because up to 84% of the product formed is propylene (Fig. 2). A tetrahedral Pt_4 cluster was used as a model for the Pt_{8-10} clusters because the three-coordinated Pt in this cluster is representative of the under-coordination of Pt found in the larger Pt_{8-10} clusters. The use of a free cluster model (without a substrate) is justified by the fact that the observed activity results for alumina and alumina/tin oxide substrates are similar (Fig. 2) and also by some model calculations done to investigate the substrate effect (see below).

The calculated transition states and intermediates in reaction channel A (formula (1)), leading to formation of propylene on the Pt_4 cluster, are shown in Fig. 3. The 'true' barrier to breaking of the first C–H bond is only 0.42 eV. The corresponding barrier referenced to gas-phase propane (the 'apparent' barrier) is slightly smaller, at 0.18 eV; this barrier was found to be similarly small (0.05 eV) when recalculated on a Pt_8 cluster. We note that, in spite of the small magnitude of the energetic barrier, this step will probably be rate-limiting because of the very large entropic loss, and consequently lower pre-exponential factor, associated with propane adsorption at high temperatures on the clusters. The rest of the pathway is thermodynamically downhill to formation of propylene, which binds to Pt_4 by its π bond. Interestingly, our calculations also indicate that dissociated oxygen atoms adsorbed on the cluster[21] do not significantly affect the calculated C–H bond activities in this pathway. In the overall reaction scheme, oxygen serves as a means for removal of hydrogen as water on the basis of these calculations.

The experimental barrier for propylene formation from propane on the subnanometre Pt clusters can be estimated to provide comparison with theory. The barrier determined from the experimental data for the $Pt_{8-10}/SnO/Al_2O_3/AAO$ catalyst at 400 and $500\,^{\circ}$C is 0.2 eV. This is consistent with the barrier found in our DFT investigation for channel A. Similarly good agreement is found when we include models for the Al_2O_3 support in our calculations. First, we considered a negatively (-1) charged Pt_4 cluster, which represents the charge transfer that occurs to the cluster when it is supported on alumina. The propane C–H reaction apparent barrier is 0.21 eV, an insignificant change from the neutral cluster. Second, we calculated the barrier for a Pt_8 cluster on a θ-alumina surface. The apparent barrier is 0.19 eV, also a small change from the result for the gas-phase Pt_8 cluster. The lack of a significant support effect is consistent with a larger binding energy per atom (~ 3 eV per atom) calculated for Pt_8 and Pt_4 clusters compared with the energy of each of the three Pt–alumina surface bonds (~ 1 eV). Although more detailed studies are needed
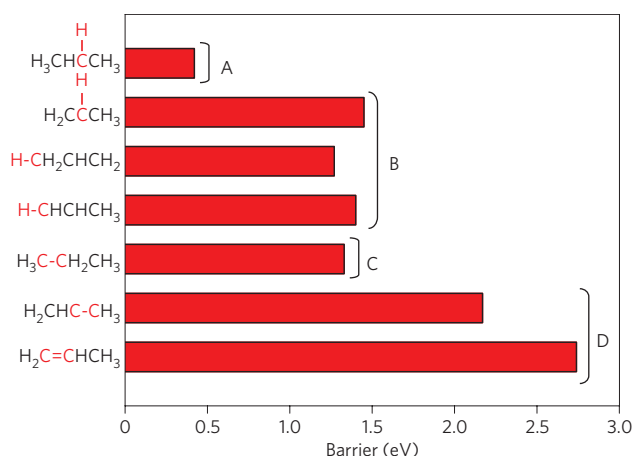

Figure 4 | Energy barriers of bond breaking. 'True' barriers for breaking C–C and C–H bonds in propane and propylene reactions on a Pt_4 cluster. Bonds that are broken are shown in red. Letters correspond to channels in formula (1). All of the barriers plotted here correspond to energies relative to the reactants (propane or propylene). In propane, the C–H bond breaking on the centre carbon (A) is favoured over a terminal carbon. In propylene C–H bond breaking all three sites (B) have similar barriers. See Supplementary Information for more details of structures and energies.

to fully elucidate the effect of the substrate, these results are strong evidence that the support has little effect on the reaction barrier in this case. In contrast to the low C–H bond scission barrier found on Pt_4, DFT calculations for C–H bond scission in propane on a Pt(111) surface give an apparent activation barrier 1 eV larger than the corresponding barrier on Pt_4. In addition, the C–H bond cleavage barriers on a supported V_2O_5 dimer are close to 1.2 eV (ref. 22) from experiment and about 2 eV from theory for a V_2O_5 surface[23].

Thus, both theory and experiment lead to the conclusion that under-coordinated Pt sites in small Pt_n clusters are much more active than a Pt surface for propane ODH. This can be explained by the attractive interaction between the under-coordinated Pt and propane. The DFT calculations show that the initial adsorption complex between propane and the Pt_4 cluster (Fig. 3) results in significant charge transfer from a propane C–H bonding orbital to the cluster. This weakens the C–H bond as demonstrated by its lengthening and a concomitant lowering of the C–H vibrational frequency by ~ 500 cm^{-1}. In contrast, propane is very weakly adsorbed on a Pt(111) surface with essentially no C–H bond lengthening or charge transfer owing to higher coordination of the surface Pt atoms.

The observed product distribution, favouring propylene formation over CO_x (84% versus 16% at $400\,^{\circ}$C—Fig. 2), suggests that C–C or C=C cleavage on the Pt clusters is less favourable than is C–H cleavage. Calculated activation barriers for various such reactions (Fig. 4) confirm this conclusion. For example, the barrier for breaking a C–C bond in propane is greater than 1 eV. In addition, propylene itself is relatively unreactive; the barriers for C–C and C=C breaking range from 2.2–2.7 eV. In addition, the barrier to break a C–H bond in the methyl group of adsorbed propylene is quite large (1.27 eV). The relatively large magnitude of this barrier is due to the considerable structural rearrangement required for the methyl group in propylene to come in contact with the Pt_4 cluster. These results, taken together, indicate that propylene will be easily formed, but other by-products, such as allene and CO_x, will not form easily.

The calculated selectivity trends can be understood from the electronic structures of the C–C and C–H bond-breaking transition states. The larger barriers observed for C–C versus C–H bond breaking are probably due to the sp^3 directionality of the orbitals on C compared with the spherical nature of the orbital on hydrogen,

which results in poorer overlap between the adsorbate and the reaction site orbitals in the transition state for breaking the C–C bond compared with that for the C–H bond. This argument has been put forward by Blomberg *et al.* for other surface reactions[24]. Computations indicate that CH_4 (ref. 25) and H_2 (ref. 26) have a small barrier and no barrier, respectively, for dissociation on a Pt_4 cluster, which supports the overlap explanation.

To our knowledge, the work reported here is the first investigation of size-preselected Pt clusters under realistic high-temperature catalytic conditions. It has revealed a very high activity of subnanometre Pt-cluster-based catalysts for the ODH of propane to propylene. Combined with quantum chemical studies, this work has shown that the high activity is due to the under-coordination of the Pt in the clusters and that the clusters favour the scission of C–H bonds relative to C–C or C=C bonds. Some recent work in our laboratory demonstrates that small gold clusters ($Au_{6–10}$) are highly active for propylene epoxidation, thus providing further evidence for the unique catalytic properties of subnanometre clusters[27]. In the future, size-selected clusters stabilized on appropriate supports with uniform surface chemistry hold great promise for design of new catalytic materials. It will be a challenging task to scale up the production of size-selected clusters by more conventional chemical methods, but there are very encouraging efforts suggesting that this will ultimately be possible[2,3].

Methods

Production of narrow cluster size distributions. The clusters emerging from the continuous beam cluster source possess identical velocity. Owing to the variation in their kinetic energy with size, in addition to the single mass selection on a quadrupole mass filter, narrow distributions of clusters with one to four sizes can be isolated using a quadrupole deflector operated in energy filter mode.

Determination of the fraction of clusters in the pores acting as active catalysts. As only 10.5% of the facing area of the membrane was exposed to clusters, and to the propane feed, a multiplication factor of 9.5 is applied to obtain the corrected propane conversion rate on the Pt-cluster-coated fraction of the AAO membrane. By calculating the relative pore opening area to the total surface area of the membrane, 28% of the $Pt_{8–10}$ particles, corresponding to 252 ng of Pt metal, enter the pores. The rest forms metallic platinum on the face of the AAO membrane as confirmed by X-ray photoemission spectroscopy. Metallic Pt is known to possess orders of magnitude lower TOFs for ODH of propane[28]. Thus, 252 ng of Pt was used for the calculation of the TOFs.

Activation barrier calculation from the experimental data. Using Arrhenius law and assuming that the conversion rate is roughly proportional to the fraction of activated C–H bonds, an estimate was obtained of the activation barrier from two available experimental values for $Pt_{8–10}/SnO/Al_2O_3/AAO$ catalyst at different temperatures.

Theoretical methods. The calculations were done using the B3LYP functional with the LANL2DZ basis set for Pt and 6-31G* for Al, C, H and O. The Pt(111) results were obtained with plane-wave calculations using the RPBE functional. See Supplementary Information for more details.

References

1. Xu, Z. *et al.* Size-dependent catalytic activity of supported metal clusters. *Nature* **372**, 346–348 (1994).
2. Gates, B. C. Supported metal clusters: Synthesis, structure, and catalysis. *Chem. Rev.* **95**, 511–522 (1995).
3. Argo, A. M., Odzak, J. F., Lai, F. S. & Gates, B. C. Observation of ligand effects during alkene hydrogenation catalysed by supported metal clusters. *Nature* **415**, 623–623 (2002).
4. Fu, Q., Saltsburg, H. & Flytzani-Stephanopoulos, M. Active Nonmetallic Au and Pt species on ceria-based water-gas shift catalysts. *Science* **301**, 935–938 (2003).
5. Campbell, C. T. The active site in nanoparticle gold catalysis. *Science* **306**, 234–235 (2004).
6. Chen, M. S. & Goodman, D. W. The structure of catalytically active gold on titania. *Science* **306**, 252–255 (2004).
7. Lemire, C., Meyer, R., Shaikhutdinov, S. & Freund, H.-J. Do quantum size effects control CO adsorption on gold nanoparticles? *Angew. Chem. Int. Ed.* **43**, 118–121 (2004).
8. Wei, J. & Iglesia, E. Mechanism and site requirements for activation and chemical conversion of methane on supported Pt clusters and turnover rate comparisons among noble metals. *J. Phys. Chem. B* **108**, 4094–4103 (2004).
9. Hvolbaek, B. *et al.* Catalytic activity of Au nanoparticles. *Nano Today* **2**, 14–18 (2007).
10. Hutchings, G. J., Scurrell, M. S. & Woodhouse, J. R. Oxidative coupling of methane using oxide catalysts. *Chem. Soc. Rev.* **18**, 251–283 (1989).
11. Labinger, J. A. & Bercaw, J. E. Understanding and exploiting C–H bond activation. *Nature* **417**, 507–509 (2002).
12. Cavani, F., Ballarini, N. & Cericola, A. Oxidative dehydrogenation of ethane and propane: How far from commercial implementation? *Catal. Today* **127**, 113–131 (2007).
13. Benz, L. *et al.* Landing of size-selected Ag_n^+ clusters on single crystal TiO_2 (110)-(1 × 1) surfaces at room temperature. *J. Chem. Phys.* **122**, 081102 (2005).
14. Lee, S., Fan, C., Wu, T. & Anderson, S. L. CO oxidation on Au_n/TiO_2 catalysts produced by size-selected cluster deposition. *J. Am. Chem. Soc.* **126**, 5682–5683 (2004).
15. Winans, R. E. *et al.* Reactivity of supported platinum nanoclusters studied by *in situ* GISAXS: Clusters stability under hydrogen. *Top. Catal.* **39**, 145–149 (2006).
16. Yoon, B. *et al.* Charging effects on bonding and catalyzed oxidation of CO on Au_8 clusters on MgO. *Science* **307**, 403–407 (2005).
17. Sadykov, V. A. *et al.* Oxidative dehydrogenation of propane over monoliths at short contact times. *Catal. Today* **61**, 93–99 (2000).
18. Pellin, M. J. *et al.* Mesoporous catalytic membranes: Synthetic control of pore size and wall composition. *Catal. Lett.* **102**, 127–130 (2005).
19. Bell, A. T. The impact of nanoscience on heterogeneous catalysis. *Science* **299**, 1688–1691 (2003).
20. Somorjai, G. A., Contreras, A. M., Montano, M. & Rioux, R. M. Cluster chemistry and dynamics special feature: Clusters, surfaces, and catalysis. *Proc. Natl Acad. Sci.* **103**, 10577–10583 (2006).
21. Xu, Y., Shelton, W. A. & Schneider, W. F. Thermodynamic equilibrium compositions, structures, and reaction energies of Pt_xO_y ($x = 1–3$) clusters predicted from first principles. *J. Phys. Chem. B* **110**, 16591–16599 (2006).
22. Argyle, M. D., Chen, K., Bell, A. T. & Iglesia, E. Effect of catalyst structure on oxidative dehydrogenation of ethane and propane on alumina-supported vanadia. *J. Catal.* **208**, 139–149 (2002).
23. Redfern, P. C. *et al.* Quantum chemical study of mechanisms for oxidative dehydrogenation of propane on vanadium oxide. *J. Phys. Chem. B* **110**, 8363–8371 (2006).
24. Blomberg, M. R. A., Siegbahn, P. E. M., Nagashima, U. & Wennerberg, J. Theoretical study of the activation of alkane C–H and C–C bonds by different transition metals. *J. Am. Chem. Soc.* **113**, 424–433 (1991).
25. Xiao, L. & Wang, L. Methane activation on Pt and Pt_4: A density functional theory study. *J. Phys. Chem. B* **111**, 1657–1663 (2007).
26. Cruz, A., Bertin, V., Poulain, E., Benitez, J. I. & Castillo, S. Theoretical study of the H_2 reaction with a Pt_4 (111) cluster. *J. Chem. Phys.* **120**, 6222–6225 (2004).
27. Lee, S. *et al.* Selective propene epoxidation on immobilized $Au_{6–10}$ clusters: The effect of hydrogen and water on selectivity and activity. *Angew. Chem. Int. Ed.* (in the press, 2008) <http://dx.doi.org/10.1002/anie.200804154>.
28. Yu, C., Xu, H., Ge, Q. & Li, W. Properties of the metallic phase of zinc-doped platinum catalysts for propane dehydrogenation. *J. Mol. Catal. A* **266**, 80–87 (2007).
29. Silberova, B., Fathi, M. & Holmen, A. Oxidative dehydrogenation of ethane and propane at short contact time. *Appl. Catal. A* **276**, 17–28 (2004).

Acknowledgements

Additional information

Subnanometer Platinum Clusters as Highly Active and Selective Catalysts for the Oxidative Dehydrogenation of Propane

Stefan Vajda*, Michael J. Pellin, Jeffrey P. Greeley, Christopher L. Marshall,
Larry A. Curtiss*, Gregory A. Ballentine, Jeffrey W. Elam, Stephanie Catillon-Mucherie, Paul C. Redfern,
Faisal Mehmood, and Peter Zapol

*e-mail: vajda@anl.gov, curtiss@anl.gov

Supplemental Information

Table of Contents

Supplemental Methods

Experimental methods: calculation of turn-over frequencies

1. Turn-over frequency calculations for catalyst reported in the literature.
For a uniform comparison, the TOF was calculated as the number of propylene molecules produced per Pt atom per time unit (seconds). Only very few TOF data were reported in the literature. In the case of the other catalysts referred in the Manuscript and in the Supplemental, the TOF was calculated based on the reported amount of catalyst used, metal loading, gas flow and gas composition data, conversion efficiency and selectivity towards propylene formed. In the case of monolith based catalysts, the geometry of the monolith substrate was also taken into consideration. As part of the calculations, space velocities were calculated as well.

2. Turn-over frequency calculations for the Pt_{8-10}/AAO catalysts.
For a uniform comparison with reported catalysts, the TOF was calculated as the number of propylene molecules produced per Pt atom per time unit (seconds) as follows:
   a. Determination of the total amount of deposited metal.
      During cluster deposition, the flux of positively charged clusters reaching the AAO surface is monitored by using a picoampermeter (Supplemental Figure 2). In the knowledge of the cluster size, the over time accumulated charge is used to calculate the number of Pt atoms (and the total mass of Pt).
   b. Determination of the fraction of Pt metal landing in the channels of the AAO membrane.
      The surface plates of the AAO membranes used were imaged by SEM (see Supplemental Figure 4) and the area fraction of the channel openings was determined.
   c. At the high level of applied coverage of the surface with clusters calculated from the deposition flux data per flat surface area and known from own earlier deposition experiments on flat surfaces, aggregation of the originally small Pt clusters on the front surface of the membrane into large nanoparticles and films was expected. XPS confirmed the presence of metallic platinum on the front surface of the membrane. It is known from literature, that Pt films/surfaces are not reactive under our relatively mild conditions or primarily cause cracking of the feedstock in films and large nanoparticles.
   d. Based on the above, for the calculation of the turn-over frequencies of the Pt_{8-10}/AAO catalysts, the amount of Pt metal directly landing in the AAO channels was taken into consideration (see Manuscript and Supplemental).

Theoretical methods.

The cluster calculations on Pt_4 and Pt_8 were carried out with the Gaussian03 code.[1] B3LYP[2,3] density functional theory4 was used for the cluster calculations with a general basis set consisting of 6-31G*[5,6] on C, H and O and LANL2DZ[7] on Pt. We used 6d functions to be consistent with the standard 6-31G* basis set. Transition states were located with QST2 and QST3 Synchronous Transit-Guided Quasi-Newton (STQN) methods as implemented in the Gaussian03 code.

The periodic calculations on Pt(111) were carried out with DACAPO, a total energy calculation code.[8] For periodic cluster calculations, a large, asymmetric unit cell (14.4x18x12Å) was used; and the reciprocal space was sampled at the gamma **k**-point. All cluster calculations were spin-optimized. For calculations on the (111) surface, a 3-layer slab with 10 layers of vacuum between any two successive metal slabs, was used. A (3x3) unit cell was employed, and the top metal layer of the slab was allowed to relax. Six Chadi-Cohen **k**-points were used. Adsorption was allowed on only one of the two surfaces exposed, and the electrostatic potential was adjusted accordingly.[9] Transition states for C-H bond cleavage in propane on the (111) surface were located with the Climbing Image Nudged Elastic Band algorithm.[10] For both cluster and periodic calculations, ionic cores were described by ultrasoft pseudopotentials,[11] and the Kohn-Sham one-electron valence states were

expanded in a basis of plane waves with kinetic energy below 340 eV; a density cutoff of 500 eV was used. The exchange-correlation energy and potential was described self-consistently within the generalized gradient approximation (GGA-RPBE).[8] The self-consistent RPBE density was determined by iterative diagonalization of the Kohn-Sham Hamiltonian, Fermi population of the Kohn-Sham states ($k_BT = 0.01$ eV for the clusters and 0.1 eV for the (111) surfaces), and Pulay mixing of the resulting electronic density.[12] The planewave PW91 results reported in the supplemental information were obtained non-self consistently with the RPBE-optimized geometries. All total energies were extrapolated to $k_BT = 0$ eV.

A comparison of selected binding energies using different methods is given in Supplemental Table 4. Included in this table are results from Gausssian basis sets and plane waves and three functionals (B3LYP, RPBE, PW91). The results show reasonable agreement among the methods.

References

1. Frisch, M. J. *et al., Gaussian 03*. (Gaussian, Inc., Wallingford CT, 2004).
2. Becke, A. D., Density-functional thermochemistry 3: The role of exact exchange. *J. Chem. Phys.* **98**, 5648 (1993).
3. Stephens, P. J., Devlin, F. J., Chabalowski, C. F. & Frisch, M. J., Ab-initio calculation of vibrational absorption and circular-dichroism spectra using density-functional force-fields. *J. Chem. Phys.* **98**, 11623 (1994).
4. Greeley, J., Nørskov, J. K. & Mavrikakis, M., Electronic structure and catalysis on metal surfaces. *Ann. Rev. Phys. Chem.* **53**, 319 (2002).
5. Hariharan, P. C. & Pople, J. A. *Theo. Chim. Acta* **28**, 213 (1973).
6. Francl, M. M. *et al.,* Self-consistent molecular-orbital methods 23: A polarization-type basis set for 2nd-row elements. *J. Chem. Phys.* **77**, 3654 (1982).
7. Hay, P. J. & Wadt, W. R., Abinitio effective core potentials for molecular calculations - potentials for k to au including the outermost core orbitals. *J. Chem. Phys.* **82**, 299 (1985).
8. Hammer, B., Hansen, L. B. & Nørskov, J. K., Improved adsorption energetics within density-functional theory using revised perdew-burke-ernzerhof functionals. *Phys. Rev. B* **59**, 7413 (1999).
9. Bengtsson, L., Dipole correction for surface supercell calculations. *Phys. Rev. B* **59**, 12301-12304 (1999).
10. Henkelman, G. & Jónsson, H., Improved tangent estimate in the nudged elastic band method for finding minimum energy paths and saddle points. *J. Chem. Phys.* **113**, 9978 (2000).
11. Vanderbilt, D., Soft self-consistent pseudopotentials in a generalized eigenvalue formalism. *Phys. Rev. B* **41**, 7892 (1990).
12. Kresse, G. & Furthmuller, J., Efficiency of ab-initio total energy calculations for metals and semiconductors using a plane-wave basis set. *Comput. Mater. Sci.* **6**, 15(1996).

Supplemental Table 1. Performance of the Pt_{8-10} cluster based and the best reported platinum and vanadia based reference ODH catalysts. A) Performance of the $Pt_{8-10}/Al_2O_3/AAO$ and $Pt_{8-10}/SnO/Al_2O_3/AAO$ catalysts as a function of temperature and location of Pt-clusters on the membrane. B) Performance of the reference ODH catalysts. Conversion* and selectivity$ data on the Pt-based catalyst were obtained from the paper of Silberova [13]et al., the turnover frequencies were calculated using metal loading and monolith geometry data communicated by A. Holmen. Selectivities& of the alumina supported VOx based catalysts were obtained from Figure 7 published by Argyle et al. [14], the turnover frequencies were calculated from the turnover rates shown in Figure 4 of the same article. The AAO membranes were positioned in the test reactor with Pt_{8-10} clusters on the entrance[x] or exit[xx] site of the channels of the AAO membrane with respect the gas flow.

Sample	Metal loading	T	Selectivity					TOF C_3H_6 molecules produced per metal atom	TOF C_3H_6 molecules produced per Pt cluster	Space velocity C_3H_8 molecules per metal atom
			C_3H_8 conversion	C_3H_6	CO_2	CO	Cracked C_xH_y products			
		(°C)	(%)	(%)	(%)	(%)	(%)	(s⁻¹)	(s⁻¹)	(s⁻¹)
A) Pt/AAO										
$Pt_{8-10}/Al_2O_3/AAO$	Pt on exit[xx]	550	25.7	68.0	32	0	0	2.9	26.4	15.1
$Pt_{8-10}/SnO/Al_2O_3/AAO$	Pt on exit[xx]	400	6.7	83.7	16.3	0	0	0.8	7.5	15.1
	Pt on entrance[x]	400	6.7	76.5	23.5	0	0	0.7	5.2	15.1
$Pt_{8-10}/SnO/Al_2O_3/AAO$	Pt on exit[xx]	500	21.9	64.0	15.7	20.3	0	2.2	19.7	15.1
	Pt on entrance[x]	500	21.9	64.3	16.4	19.3	0	2.2	19.5	15.1
	entrance, 14 hrs[x]	500	21.9	65.2	15.6	19.2	0	2.2	19.9	15.1
B) Reference ODH										
Pt on monolith [13]		400	12.5*	5$	30$	60$	5$	1.76×10^{-2}[#]		25
		550	15.0*	6$	19$	75$	0$	2.25×10^{-1}[#]		25
VOx/Al_2O_3 [14]	1.4 V nm⁻²	390	Extrapolated to zero C_3H_8 conversion [14]	87.0 &	4.5 &	8.5 &	0	1.70×10^{-3}		Extrapolated to zero space velocity [14]
	8.0 V nm⁻²	390		82.2 &	4.8 &	13.0 &	0	7.80×10^{-3}		
	16.6 V nm⁻²	390		79.0 &	6.5 &	14.5 &	0	3.60×10^{-3}		
	34.2 V nm⁻²	390		71.5 &	7.5 &	21.0 &	0	1.90×10^{-3}		

13. Silberova B., Fathi M. & Holmen A., Oxidative dehydrogenation of ethane and propane at short contact time. *Appl. Catal. A: General* **276**, 17 (2004).

14. Argyle M. D., Chen K., Bell A. T. & Iglesia E., Effect of Catalyst Structure on Oxidative Dehydrogenation of Ethane and Propane on Alumina-Supported Vanadia *J. Catal.* **208**, 139 (2002).

SUPPLEMENTARY INFORMATION

Supplemental Table 2. Performance of other reported platinum based propane ODH catalysts. In cases where turnover frequencies and space velocities were reported using different units or not provided directly, the data shown in the table were calculated using the reported metal loading, catalyst geometry and gas flow data. The turnover frequencies[#] from ref.[16] were calculated using metal loading and monolith geometry data communicated by A. Holmen.

Sample/reference		T	Selectivity					TOF C_3H_6 molecules produced per metal atom	TOF C_3H_6 molecules produced per Pt cluster	Space velocity C_3H_8 molecules per metal atom
			C_3H_8 conversion	C_3H_6	CO_2	CO	Cracked C_xH_y products			
		(ºC)	(%)	(%)	(%)	(%)	(%)	(s⁻¹)	(s⁻¹)	(s⁻¹)
Fathi et al. [15]		800	24	25	25	25	25	3.11×10^{-2}	-	0.51
Pt/10% Rh gauze		840	46	28	10	15	45	6.67×10^{-2}	-	0.51
		860	58	26	6	11		7.81×10^{-2}	-	0.51
		890	74	22	5	16	57	8.43×10^{-2}	-	0.51
		920	92	12	2	18	63	5.72×10^{-2}	-	0.51
Silberova et al. [16]		400	12.5	5	30	60	5	1.76×10^{-2} [#]	-	25
Pt/monolith		550	15	6	19	75	0	2.25×10^{-1} [#]	-	25
		850	71	18	2	25	40	3.19 [#]	-	25
Sadykov et al. [17]										
Pt/α-Al₂O₃	Sn/Al 0.1/0.29	835	63	17.5	2.7	21	52	3.67	-	33.3
Pt-SnO₂/αAl₂O₃+SiO2		850	47	26.4	28.5	2.5	35.2	1.24	-	10
Pt-SnO₂/α-Al₂O₃+SiO₂	Prop to O2 1:1	700	20	19	70	-	5	1.93	-	10
	Prop to O2 3:1	700	55	35	5	-	30	9.8	-	10
Pt-SnO₂/α-Al₂O₃+SiO₂	Sn/Al 0.04/0.02	840	61.5	20.6	11.5	15.2	44	1.26	-	10
Pt-SnO₂/ZnAl₂O₃	Sn/Al 0.56/9	880	32.6	25.3	45	10	17.6	8.24×10^{-1}	-	10
Beretta et al. [18]		450	20	0	98	2	0	0	-	8.25
Pt/Al2O3		500	20	0	95	5	0	0	-	8.25
		550	24	2.2	80	17.8	0	2.69×10^{-1}	-	8.25
		625	39	28	20	20	23.4	5.48	-	8.25
		650	60	20	25	23	32	6.12	-	8.25

15. Fathi, M., Lodeng, R., Nilsen ,E. S., Silberova, & B. Holmen A., Short contact time oxidative dehydrogenation of propane. *Catal. Today* **64**, 113 (2001).
16. Silberova, B., Fathi, M. & Holmen, A., Oxidative dehydrogenation of ethane and propane at short contact time. *Appl. Catal. A: General* **276**, 17 (2004).
17. Sadykov, V. A. *et al.*, Oxidative dehydrogenation of ethane and propane at short contact time. *Catal. Today* **61**, 93 (2000).
18. Beretta, A., Piovesan, L. & Forzatti, P., Production of olefins via oxidative dehydrogenation of propane in autothermal conditions. *J. Catal.* **184**, 455 (1999).

Supplemental Table 3. Performance of reported platinum based propane DH catalysts. In cases where turnover frequencies and space velocities were reported using different units or not provided directly, the data shown in the table were calculated using the reported metal loading, catalyst geometry and gas flow data.

Sample/reference		T		Selectivity			Cracked C_xH_y products	TOF in C_3H_6 molecules produced per metal atom	TOF in C_3H_6 molecules produced per Pt_8 center	Space velocity in C_3H_8 molecules per metal atom
			C_3H_8 conversion	C_3H_6	CO_2	CO				
		(°C)	(%)	(%)	(%)	(%)	(%)	(s⁻¹)	(s⁻¹)	(s⁻¹)
Yu et al. [19]	C_3H_8:H_2:Ar 1:1:5	576	45	98	N/A	N/A	N/A	6.61×10^{-2}	-	0.15
Pt-Ce-Zn/□-Al2O3		576	43	64	N/A	N/A	N/A	4.12×10^{-2}	-	0.15
Pt-Ce/γ-Al2O3		576	37	96	N/A	N/A	N/A	5.32×10^{-2}	-	0.15
Pt-Zn/γ-Al2O3		576	34	79	N/A	N/A	N/A	4.03×10^{-2}	-	0.15
Pt/γ-Al2O3		576	45	98	N/A	N/A	N/A	6.61×10^{-2}	-	0.15
De Cola et al. [20]	C_3H_8									
0.5Pt/Na-Beta, t=1h		555	36	57	N/A	N/A	N/A	1.48×10^{-4}	-	2.6
0.5Pt/Na-Beta, t=12h		555	5	68	N/A	N/A	N/A	2.46×10^{-5}	-	2.6
0.5Pt/2.6ZnBeta, t=1h		555	40	57	N/A	N/A	N/A	5.32×10^{-2}	-	2.6
0.5Pt/2.6ZnBeta,t=12h		555	30	90	N/A	N/A	N/A	4.03×10^{-2}	-	2.6
Barias et al. [21]										
Pt /Al2O3	C_3H_8:N_2 3: 7	427	N/A		N/A	N/A	N/A	0.8	-	10
Pt-Sn/Al2O3	C_3H_8:N_2 3: 7	427	N/A		N/A	N/A	N/A	1.2	-	10
Pt /Al2O3	C_3H_8:N_2 3: 7	519	N/A		N/A	N/A	N/A	1	-	10
Pt-Sn/Al2O3	C_3H_8:N_2 3: 7	519	N/A	84	N/A	N/A	N/A	3.8	-	10
Pt/Al2O3	C_3H_8:N_2:H_2 3:7:1	519	N/A	94	N/A	N/A	N/A	0.6	-	3.3
Pt-Sn/Al2O3	C_3H_8:N_2:H_2 3:7:1	519	N/A	94	N/A	N/A	N/A	0.6	-	3.3
Waku et al. [22]										
Pt /Na-(Fe)-ZSM5		520	35.5	96.9			3.1	1.4	-	4.1
		520	31.2	98.9			2.1	5.0	-	16.2
		520	18.9	99.6			0.4	14.8	-	78.7

19. Yu, C., Ge, Q., Xu, H. & Li, W., Effects of Ce addition on the Pt-Sn/γ-Al₂O₃ catalyst for propane dehydrogenation to propylene. *App. Catal. A: General* **315**, 58 (2006).
20. De Cola, P. L., Glaser & R., Weitkamp, Non-oxidative propane dehydrogenation over Pt-Zn-containing zeolites. *J. App. Catal. A: General* **306**, 85 (2006).
21. Barias, O. A., Holmen A., Blekkan E. A, Propane Dehydrogenation over Supported Pt and Pt–Sn Catalysts: Catalyst Preparation, Characterization, and Activity Measurements. *J. Catal.* **158**, 1 (1996).
22. Waku, T., Biscardib, J. A., Iglesia, E., Active, selective, and stable Pt/Na-[Fe]ZSM5 catalyst for the dehydrogenation of light alkanes. *Chem. Commun.*, 1764 (2003)

Supplemental Table 4. DFT results for selected binding energies of adsorbates on Pt_4. The planewave PW91 energies were calculated non-self consistently from RPBE-optimized geometries. All energies are reported in eV and donot include entropies. Multiplicities are given in parentheses. The results for the different methods are in general agreement.

	Reaction Energies, eV			
	Gaussian basis sets		Planewave basis sets	
Reaction	B3LYP	PW91	RPBE	PW91
$C_3H_8(1) + Pt_4(3) \rightarrow Pt_4 ---C_3H_8(3)$	-0.24	-0.48	-0.21	-0.43
$C_3H_7(2) + Pt_4(3) \rightarrow Pt_4 ---C_3H_7(2)$	-2.07	-2.50	-2.17	-2.59
$C_3H_6(1) + Pt_4(3) \rightarrow Pt_4 ---C_3H_6(3)$	-1.74	-2.19	-1.78	-2.11
$C_3H_5(2) + Pt_4(3) \rightarrow Pt_4 ---C_3H_5(2)$	-2.79	-3.40	-2.89	-3.31
$C_3H_4(1) + Pt_4(3) \rightarrow Pt_4 ---C_3H_4(3)$	-1.39	-2.06	-1.60	-2.02
$H(2) + Pt_4(3) \rightarrow Pt_4 ---H(2)$	-2.76	-3.02	-3.10	-3.18
$O(3) + Pt_4(3) \rightarrow Pt_4 ---O(3)$	-3.63	-4.86	-4.18	-4.53

Supplemental Table 5. B3LYP reaction energies and barriers for channel A based on Pt_4 that are shown in Figure 4 of the article. Energies of structures C1, C2, C5, C6, C7 are included in Figure 4 in the article. The other structures involve mainly hydrogen movement and are not shown in the figure. Energy data is relative to Pt_4 + propane. Structures are illustrated in Supplemental Figure 6. TS = transition state.

Structure	Structure Label	Relative Energy[a], eV
$Pt_4 + C_3H_8$[c]		0.00 (0.0)
$Pt_4...C_3H_8$[c]	C1	-0.24 (-0.25)
$TS[C1 \rightarrow C3]$[c]	C2	0.18
Pt_4-(H,C_3H_7) (H, C_3H_7 on same Pt site)	C3	-0.58
$TS[C3 \rightarrow C5]$	C4	-0.16
Pt_4-(H,C_3H_7) (H, C_3H_7 on different Pt sites)[c]	C5	-0.54
TS $(C5 \rightarrow C7)$[c]	C6	-0.17
Pt_4-(H,H,C_3H_6) (H, H, C_3H_6 on different Pt sites)[c]	C7	-0.95
TS $(C7 \rightarrow C9)$	C8	-0.75
Pt_4-(H,H,C_3H_6) (H, H, C_3H_7 on different Pt sites)	C9	-0.95
TS $(C9 \rightarrow C11)$	C10	-0.26
Pt_4-(H_2,C_3H_6)	C11	-0.77
Pt_4-(H_2,C_3H_6)	C12	-1.10
Pt_4-$C_3H_6 + H_2$	C13	-0.08
Pt_4-(H_2) + propylene	C14	0.37
Pt_4-(H,H) + propylene	C15	0.55
$Pt_4 + C_3H_6 + H_2$		1.67

[a] Energies are for Pt_4 structures in the triplet state (multiplicity 3), except for energies

in parentheses that are for the singlet state.
[b] The singlet state Pt_4 cluster is 0.31 eV less stable than the triplet state Pt_4 cluster.
[c] Energies included in Figure 2 in the article.

Supplemental Table 6. B3LYP reaction energies and barriers for selected reactions on Pt_8. The results are in reasonable agreement with the same reactions for Pt_4 in Supplemental Tables 4 and 5. Structures are illustrated in Supplemental Figure 7. TS = transition state.

Reaction	Structure	ΔE^a, eV
C-H bond activation		
$C_3H_8 + Pt_8 \rightarrow Pt_8$---$C_3H_8$	D1	-0.35
TS (E2 $\rightarrow$ E4)	D2	0.40 (0.05)[b]
$C_3H_8 + Pt_8 \rightarrow Pt_8$-(H,$C_3H_7$)	D3	-0.60
Other structures for H and C_3H_7 attachment		
$C_3H_8 + Pt_8 \rightarrow Pt_8$-(H,$C_3H_7$)	D4	-0.44
$C_3H_8 + Pt_8 \rightarrow Pt_8$-(H-$C_3H_7$)	D5	-0.51
Structures and energies for propylene adsorption		
$C_3H_6 + Pt_8 \rightarrow Pt_8$---$C_3H_6$	D6	-1.71
$C_3H_6 + Pt_8 \rightarrow Pt_8$---$C_3H_6$	D7	-1.47
$C_3H_6 + Pt_8 \rightarrow Pt_8$---$C_3H_6$	D8	-1.46

[a] Energies are for Pt cluster structures in the triplet state (multiplicity 3).
[b] Value in parentheses is relative to energy of separated species, Pt_8 and C_3H_8.

Supplemental Table 7. B3LYP activation barriers relative to reactants ("apparent barriers") and relative to the minimum corresponding to the adduct between C_3H_8 (or C_3H_6) and Pt_4 ("true barriers"). This is the data used for Figure 5 in the article. The structures involving Pt_4 are calculated as triplets in all cases. Structures are in Supplemental Figure 8.

Reaction	TS Structure	Barrier, eV	
		"apparent"	"true"
Pathway A			
$C_3H_8 + Pt_4 \rightarrow Pt_4(H,C_3H_7)$	E1	0.18	0.42
Pathway B			
$C_3H_6 + Pt_4 \rightarrow Pt_4(H,C_3H_5)^a$	E2	-0.29	1.45
$C_3H_6 + Pt_4 \rightarrow Pt_4(H,C_3H_5)^b$	E3	-0.47	1.27
$C_3H_6 + Pt_4 \rightarrow Pt_4(H,C_3H_5)^c$	E4	-0.34	1.40
$C_3H_6 + Pt_4 \rightarrow Pt_4(H,C_3H_5)^c$	E5	-0.34	1.40
Pathway C			
$C_3H_8 + Pt_4 \rightarrow Pt_4(CH_3,CH_2CH_3)$	E6	1.09	1.33
Pathway D			
$C_3H_6 + Pt_4 \rightarrow Pt_4(CH_3,CHCH_2)^d$	E7	0.43	2.17
$C_3H_6 + Pt_4 \rightarrow Pt_4(CH_2,CHCH_3)^e$	E8	1.00	2.74

[a] H is from CH group.
[b] H is from CH_3 group.
[c] H is from CH_2 group.
[d] Breaking C-C bond in propylene.
[e] Breaking C=C bond in propylene.

Supplemental Table 8. B3LYP density functional results for O_2 and O reactions with Pt_4 cluster. Structures are in given in Supplemental Figure 9. Multiplicities are given in parentheses. These results show that oxygen will likely dissociate on Pt_4 and are used in the calculations in Supplemental Table 9 investigating the effect of adsorbed oxygen on the propane reactions.

Reaction	Structure	ΔE, eV
Pt_4 (3) + O (3) $\rightarrow$ Pt_4-O (3)	F1	-3.63
Pt_4 (3) + O_2 (3) $\rightarrow Pt_4...O_2$ (5)	F2	-0.81
$TS[(Pt_4...O_2)$ (5) $\rightarrow Pt_4$-(O,O)] (5)	F3	0.81^a
Pt_4 (3)+ O_2 (3) $\rightarrow Pt_4$-(O,O) (5)	F4	-1.63

[a] "True" barrier relative to $Pt_4...O_2$. The "apparent" barrier is 0.0 eV.

Supplemental Table 9. B3LYP energies and structures for propane C-H bond breaking when oxygen is at the reaction site (G1, G2, G3) and at an adjacent site (G4, G5, G6) for the Pt_4 cluster. Structures are illustrated in Supplemental Figure 10. The structures involving Pt_4 are calculated as triplets in all cases. The results indicate that adsorbed oxygen has little effect on the C-H cleavage of propane at either the oxygen site or adjacent to it.

Reaction	Structure	ΔE, eV
Reaction at site adjacent to oxygen		
$Pt_4O + C_3H_8 \rightarrow Pt_4O\ldots C_3H_8$	G1	-0.38
TS (G1$\rightarrow$G3)	G2	0.55 (0.17)
$Pt_4O + C_3H_8 \rightarrow Pt_4O\text{-}(C_3H_7,H)$	G3	-0.44
Reaction at oxygen site		
$Pt_4O + C_3H_8 \rightarrow Pt_4O\ldots C_3H_8$	G4	-0.04
TS (G4$\rightarrow$G6) (3)	G5	0.61 (0.57)
$Pt_4O + C_3H_8 \rightarrow Pt_4O\text{-}(C_3H_7,H)$	G6	-1.31

[a]Value in parentheses is relative to energy of separated species, Pt_4 and C_3H_8, i.e. the "apparent" barrier.

Supplemental Table 10. Approximate analysis of adsorption free energies of H_2O and C_3H_6 adsorption on the Pt_4 cluster. These calculations are based on translational entropy contributions to the gas phase molecule and assuming all other entropy contributions approximately cancel or are small. Temperature effects on enthalpies are also neglected. Results are based on B3LYP calculations. The results shows that entropic effects are important and make the dissociation products (H_2O and C_3H_6) more favorable.

Reaction	ΔE_e eV	S_{trans} eV	T K	ΔTS eV	$\Delta E - \Delta TS$ eV
$Pt_4 + H_2O \rightarrow Pt_4\text{---}OH_2$	-0.92	1.67	673.2	-1.13	0.21
$Pt_4 + C_3H_6 \rightarrow Pt_4\text{---}C_3H_6$	-1.74	1.79	673.2	-1.20	-0.53

Supplemental Table 11. Selected binding energies and activation barriers on Pt(111). The TS (transition state) is referenced to gaseous propane; this value is equivalent to the "apparent" activation barrier. The barriers can be compared to B3LYP "apparent" barrier values of 0.18 and 0.05 eV for Pt_4 and Pt_8 clusters, respectively, in Supplemental Table 5 and 6. The PW91 density functional gives an "apparent" barrier for C-H bond breaking on a Pt_4 cluster of -0.25 eV as the barrier is below the energies of the reactants and, thus, seems to underestimate this barrier compared to the B3LYP. The RPBE functional gives a "true" barrier of ~0.3 eV for C-H bond breaking on Pt_4 in agreement with the B3LYP results. Thus, the RPBE results indicate that the barrier on Pt(111) is about 1 eV higher than on the cluster.

	ΔE, eV	
	RPBE	PW91[a]
Pt(111) + C_3H_8 → Pt(111)-C_3H_8	0.00	-0.04
TS[C_3H_8 →(C_3H_7,H)][b]	1.20	0.71
Pt(111) + C_3H_7 → Pt(111)-C_3H_7	-1.19	-1.66
Pt(111) + C_3H_6 → Pt(111)-C_3H_6	-0.55	-1.07
Pt(111) + C_3H_5 → Pt(111)-C_3H_5	-1.55	-2.17
Pt(111) + H → Pt(111)-H	-2.59	-2.70

[a] The PW91 energies are calculated non-self consistently from RPBE-optimized geometries.

[b] The barriers are "apparent" values relative to the reactants.
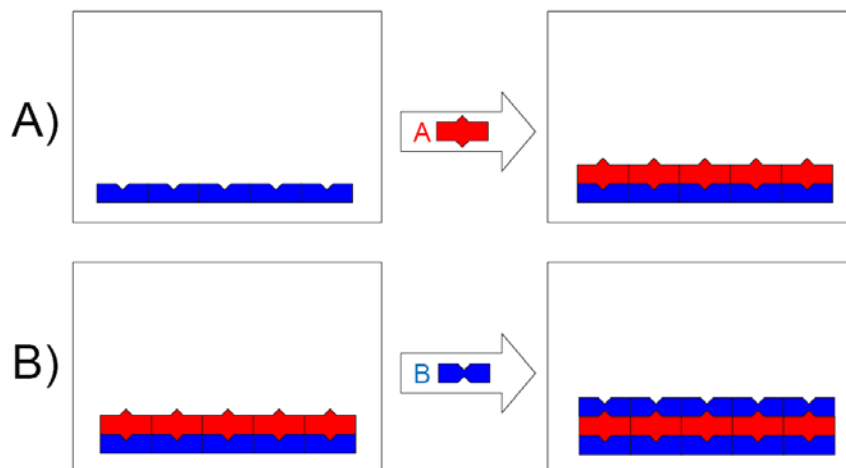
Supplemental Figure 1. Schematic illustration of ALD process. The notches in the starting substrate for reaction A represent discrete reactive sites. Exposing this surface to reactant A results in the self-limiting chemisorption of a monolayer of A species. The resulting surface becomes the starting substrate for reaction B. Subsequent exposure to molecule B covers the surface with a monolayer of B species. Consequently, one AB cycle deposits one monolayer of the compound AB and regenerates the initial substrate. By repeating the binary reaction sequence in an ABAB… fashion, films can be deposited with atomic layer precision.

Atomic Layer Deposition: Atomic layer deposition (ALD) was used to deposit both the Al_2O_3 and SnO catalytic support layers. ALD is a thin film growth technique that uses alternating cycles of saturating reactions between gaseous precursor molecules and a substrate to deposit films in a monolayer-by-monolayer fashion as illustrated in Figure 1. As a specific example, consider the ALD of Al_2O_3 using alternating exposures to trimethyl aluminum (TMA) and water(1):

$$\text{A)} \quad \text{Al-OH*} + \text{Al(CH}_3)_3 \quad \rightarrow \quad \text{Al-O-Al(CH}_3)_2\text{*} + \text{CH}_4 \tag{1}$$

$$\text{B)} \quad \text{Al-CH}_3\text{*} + \text{H}_2\text{O} \quad \rightarrow \quad \text{Al-OH*} + \text{CH}_4 \tag{2}$$

In these equations, the asterisks represent surface species, and the reactions have been simplified to show only a single functional group. In equation 1 (A cycle), a surface hydroxyl species reacts with TMA to deposit a monolayer of methyl-terminated Al atoms and liberate methane gas. In equation 2 (B cycle), the resulting surface reacts with water to restore the hydroxyl-termination and again liberate methane. The result of one AB cycle is to deposit a monolayer of Al_2O_3 on the surface and regenerate the original starting surface so that the process can be repeated. In ALD, gaseous diffusion of the reactive precursors, along with self-termination of the individual chemical reactions ensure that all surfaces of a substrate are coated uniformly even in the case of high surface area, nanoporous solids such as the AAO membranes used in this study. Consequently, ALD eliminates the "line of site" or "constant exposure" requirements that make it impossible to uniformly coat porous, high-surface-area catalyst supports using traditional physical- or chemical vapor deposition methods.

The SnO ALD was accomplished using alternating exposures to tin tetrachloride ($SnCl_4$) and water. Based on our experience, it is unlikely that the SnO will grow on top of the Pt clusters because the Pt surfaces do not poses hydroxyl groups for the $SnCl_4$ to react with. Instead, the SnO will grow on the hydroxyl-terminated A_2O_3 surfaces which surround the Pt clusters

23. Ott, A. W. Klaus, J. W. Johnson, J. M. George, S. M., Al_2O_3 thin film growth on Si (100) using binary reaction sequence chemistry, *Thin Solid Films* **292**, 135 (1997)
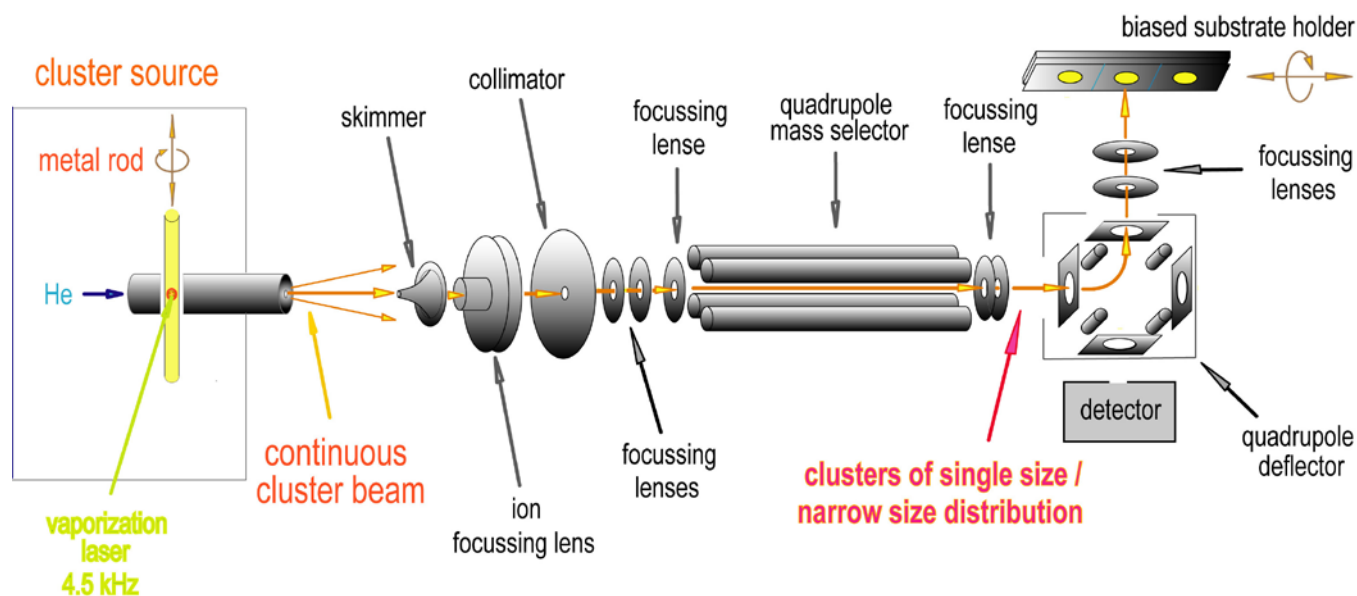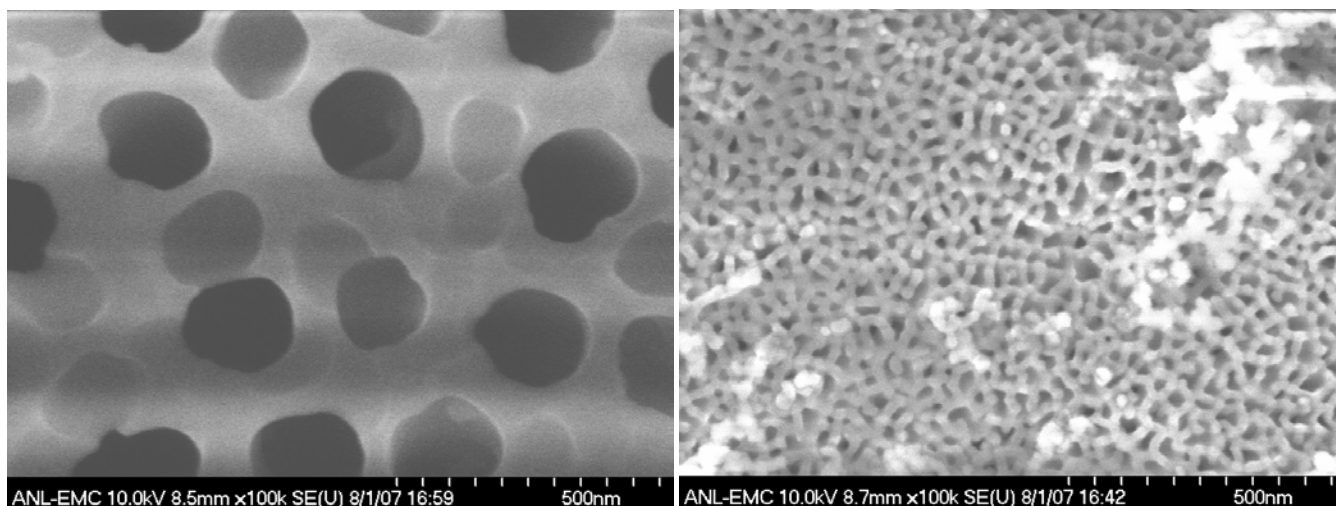
Supplemental Figure 2. Schematic of the size-selected cluster deposition setup allowing for soft-landing and controlled surface coverage. [24] The continuous beam of metal clusters is generated in a laser vaporization cluster source which utilizes a Nd:YAG laser operating at 4.5 kHz. The beam of neutral and charged platinum clusters passes through a biased skimmer into the ion guide of the second differentially pumped vacuum stage and then into the third vacuum stage. The positively charged clusters are then guided and focused into the quadrupole mass spectrometer for analysis. Narrow Pt-cluster distributions) in the mass range of up to 2000 amu can be produced by optimizing the temperature of the clusters source, pressure of the helium carrier gas and potential settings on the individual ion optics elements. After the mass analysis of the cluster distribution is completed, by reversing the polarity settings on the quadrupole deflector, the mass-selected Pt-clusters are deflected into an ion lense setup placed in front of the substrate. The substrate (a flat oxide surface or an AAO membrane) is mounted on a translation stage. By translating the support during cluster deposition, a larger area of the support can be covered by the catalytic clusters. Clusters of single size can be deposited by operating the quadrupole mass filter in a mass resolving mode. Alternatively, the quadrupole can be operated in ion-guide mode – guiding the narrow cluster size distribution towards the quadrupole deflector Using this approach, very narrow distribution of cluster sizes can be extracted from the beam when using the deflector as an energy filter (e.g. 2 to 4 dominant cluster sizes) The latter approach was implemented during the course of this study and Pt_{8-10} clusters were soft-landed on AAO membranes. The kinetic energy of clusters landing on the surface is controlled by biasing the substrate (typically 0.5 eV/atom). Low deposition energies are used to avoid possible fragmentation of clusters upon their impact on the surface (in the literature refrerred to this deposition as "soft-landing"). The flux of Pt_{8-10} clusters landing on the support was monitored in real-time using a picoampermeter. By integrating the accumulated charge of the positively charged Pt_{8-10} clusters landing on the surface, the exact surface coverage with Pt-metal is determined.

24. Vajda, S. *et al.*, Supported gold clusters and cluster-based nanomaterials: Characterization, stability and growth studies by in situ GISAXS under vacuum conditions and in the presence of hydrogen. *Top. Catal.* **39**, 161 (2006).
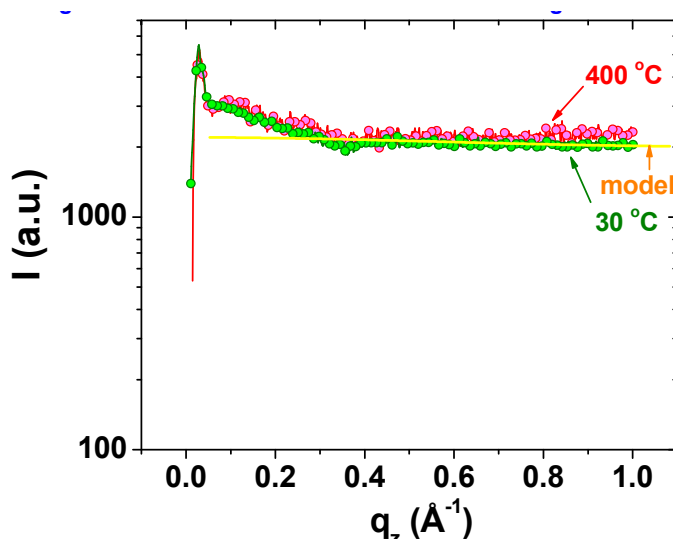
Supplemental Figure 3. Stability of Pt_{7-10} clusters on with alumina film coated flat Si-wafer at elevated temperatures. [25] The plot shows grazing incidence small angle X-ray scattering data at room temperature and after keeping the temperature at 400 ºC for several hours (scattered X-ray intensity I as a function of the scattering vector q). The two X-ray scattering signals are practically identical, thus providing a proof of absence of sintering of the Pt clusters at elevated temperatures. The straight line in the plot is the calculated scattering pattern obtained using the coordinates of a spherical Pt_{10} cluster, showing an excellent match with the experimental data. This figure is a reproduction, with kind permission from Springer Science + Business Media of Figure 6b of the paper: "Reactivity of Supported Platinum Nanoclusters Studied by In Situ GISAXS: Clusters Stability under Hydrogen" of authors R.E. Winans, S. Vajda, G.E. Ballentine, J.W. Elam, B. Lee, M.J. Pellin, S. Seifert, G.Y. Tikhonov and N. A. Tomczyk, published in *Top. Catal.,* Volume **39**, page 145 (2006), and any original (first) copyright notice displayed with material.

25. Winans, R E. *et al.*, Reactivity of supported platinum nanoclusters studied by in situ GISAXS: Clusters stability under hydrogen. *Top. Catal.* 39, 149 (2006).

Supplemental Figure 4. SEM of the AAO membranes used: Large pore side (left) and small pore side (right). Clusters were deposited on the large pore side of the membrane.
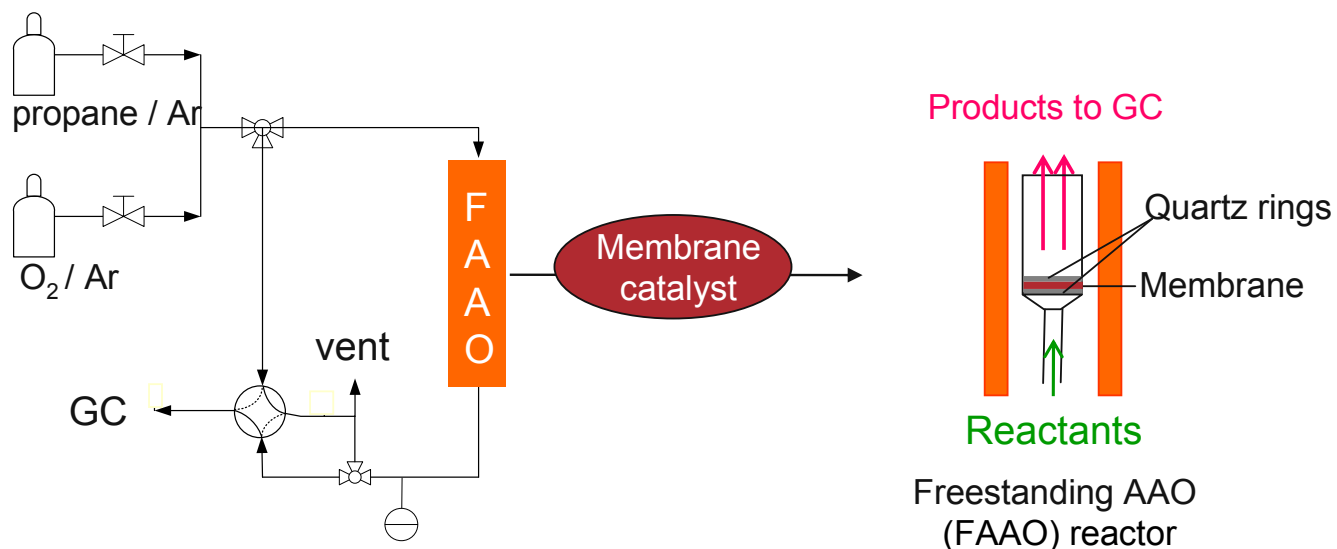
Supplemental Figure 5. Schematic of the freestanding AAO (FAAO) flow reactor setup for catalyst tests. By reversing the AAO membrane, the catalytically active particles will be at the entrance or at exit of the pores. The catalysts' tests were performed at temperatures up to 550 ºC and the products formed were analyzed by on-line gas chromatography (GC).
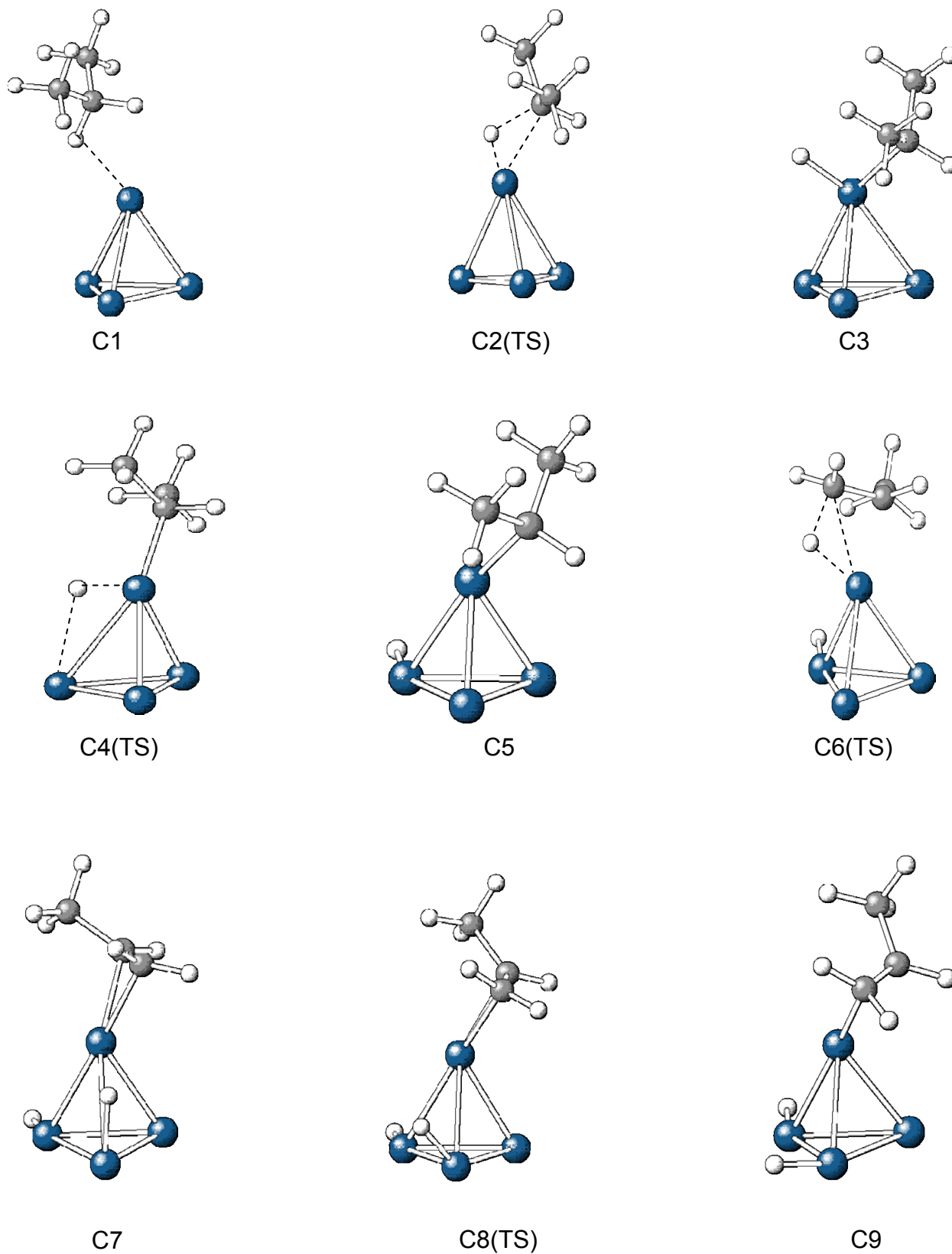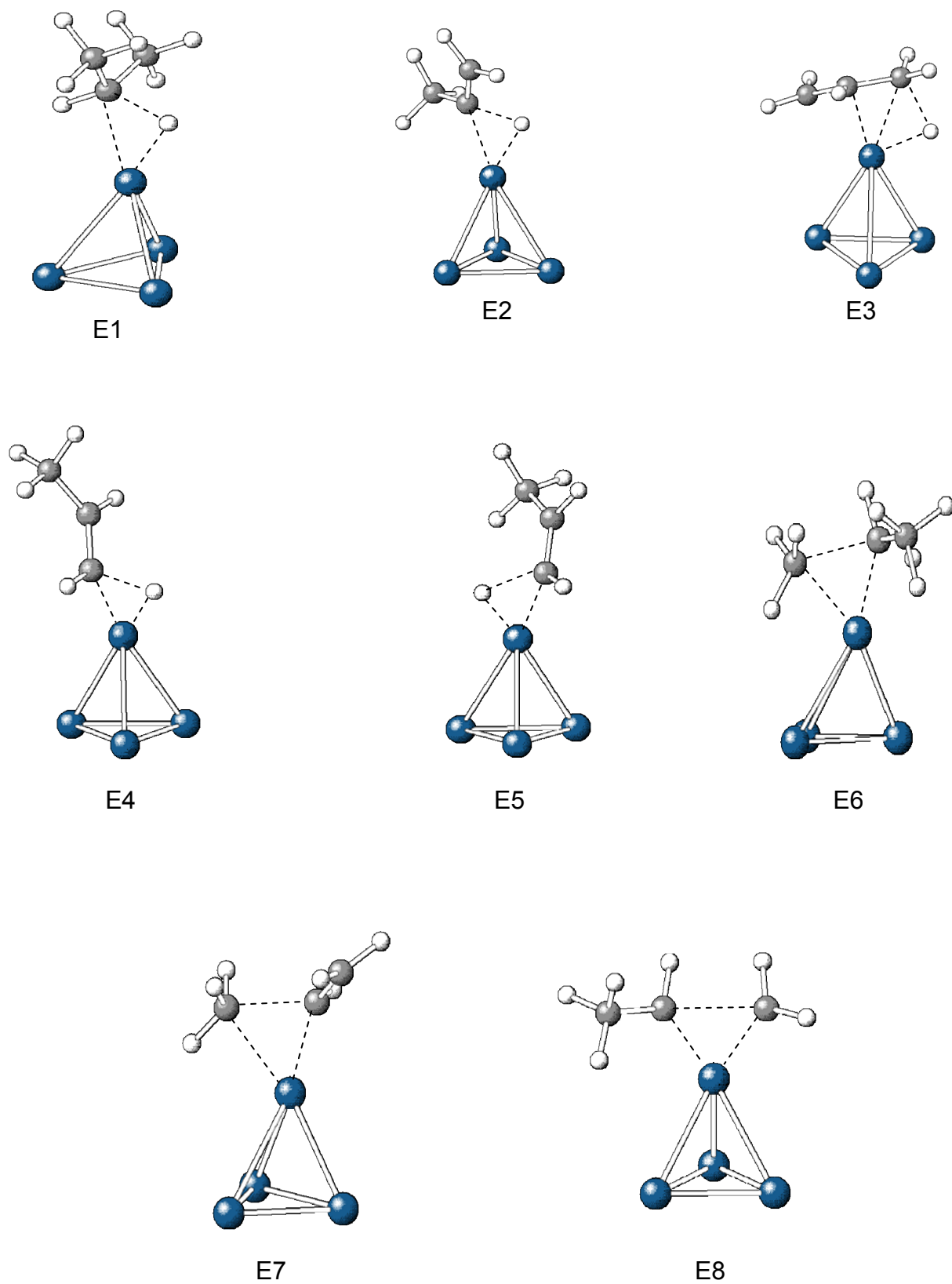
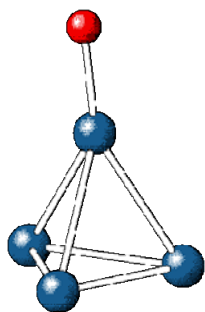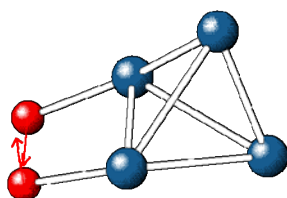**Supplemental Figure 6.** B3LYP structures for energies in Supplemental Table 5.

C10(TS)

C11

C12

C13

C14

C15
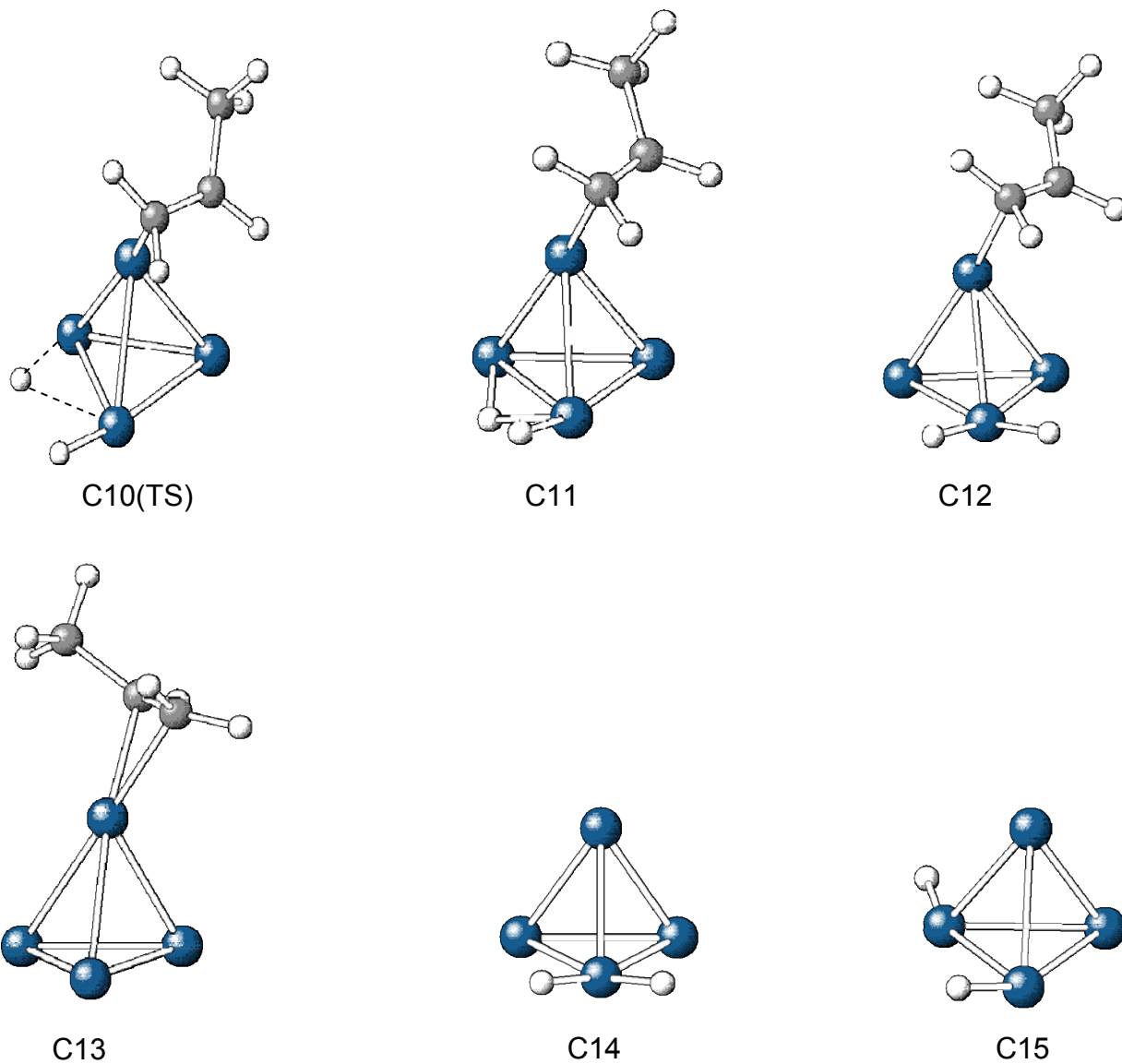
Supplemental Figure 6 (continued). B3LYP structures for energies in Supplemental Table 5.
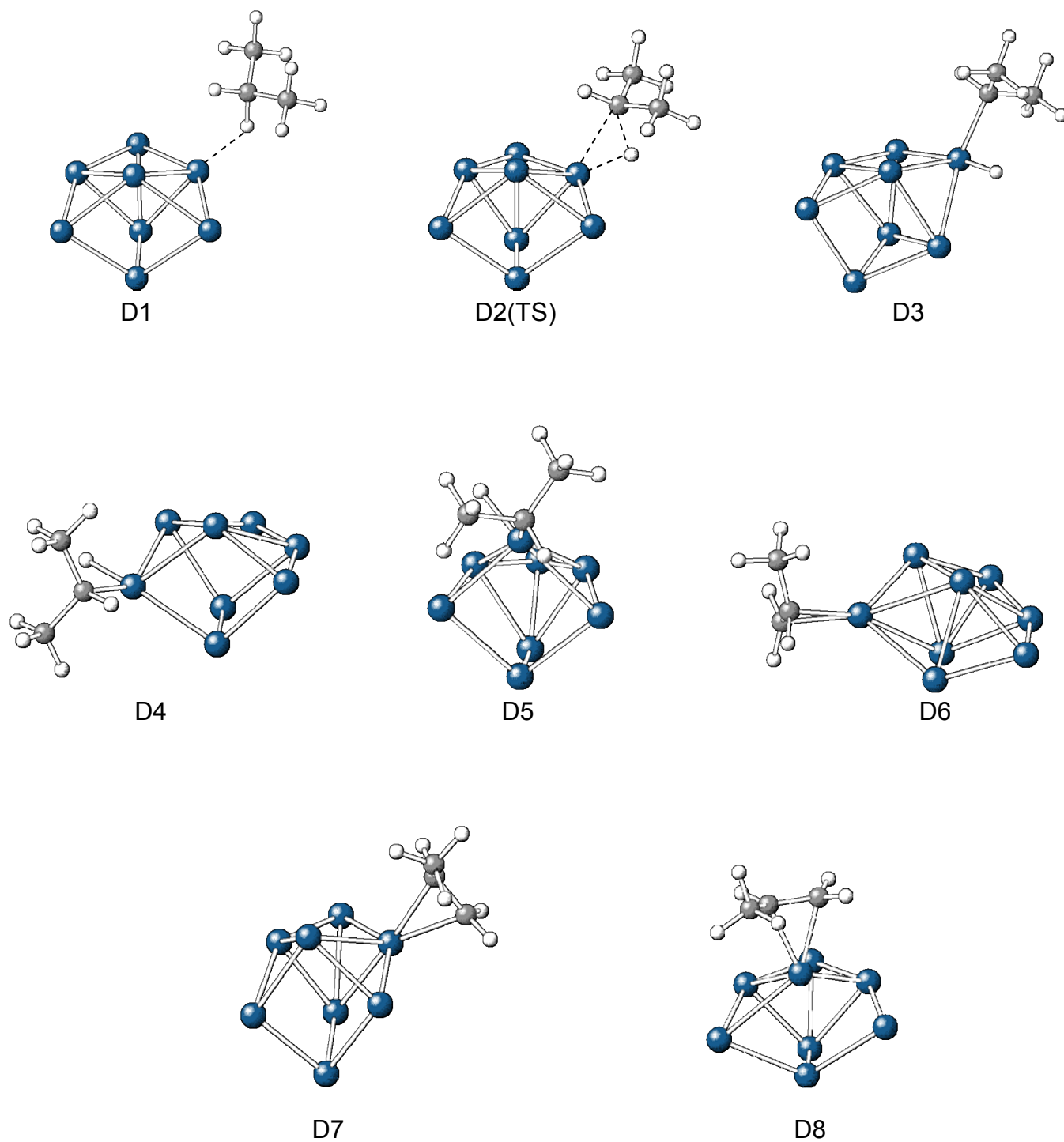
Supplemental Figure 7 B3LYP structures for energies in Supplemental Table 6.

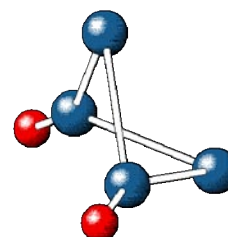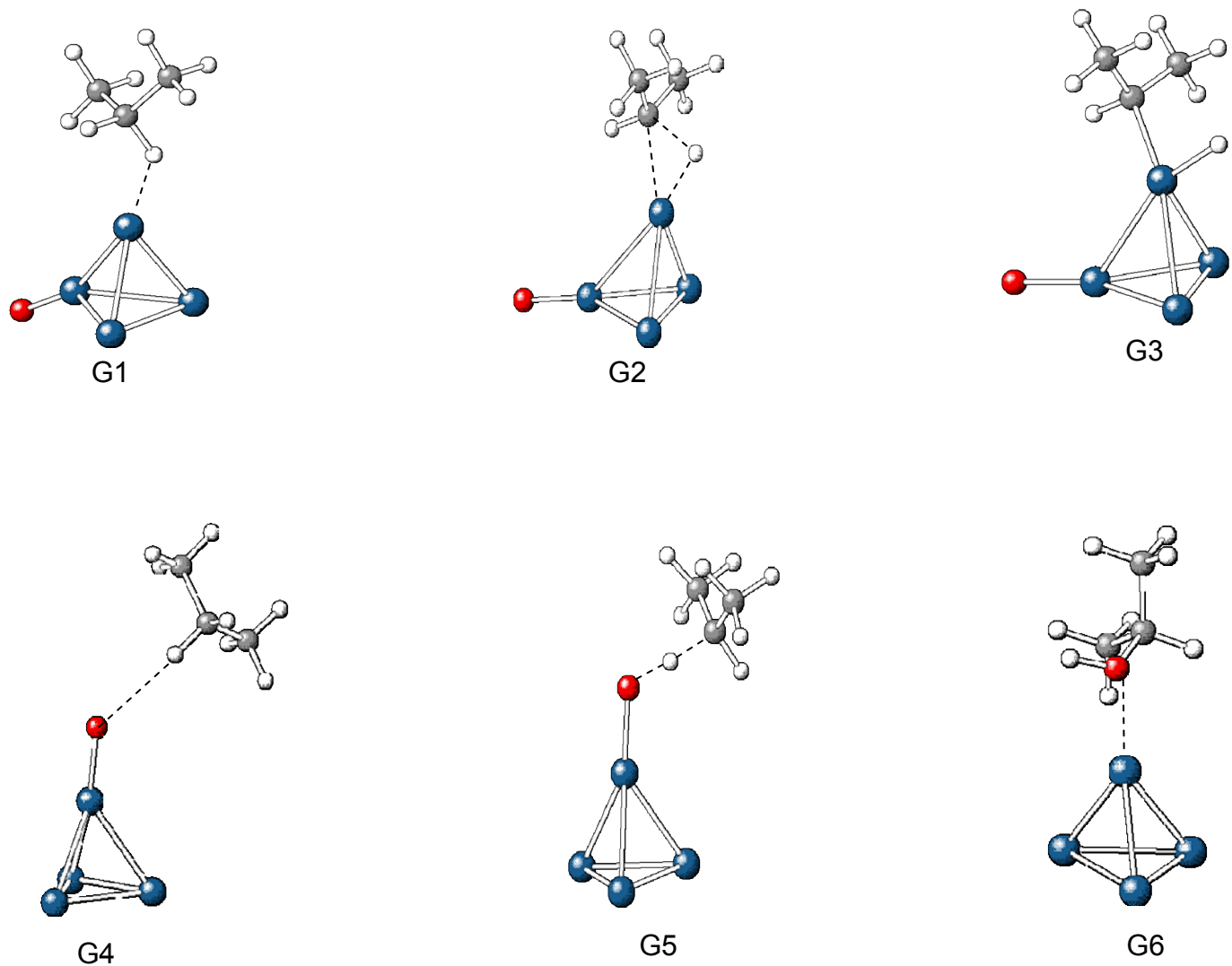**Supplemental Figure 8.** B3LYP structures for energies in Supplemental Table 7.
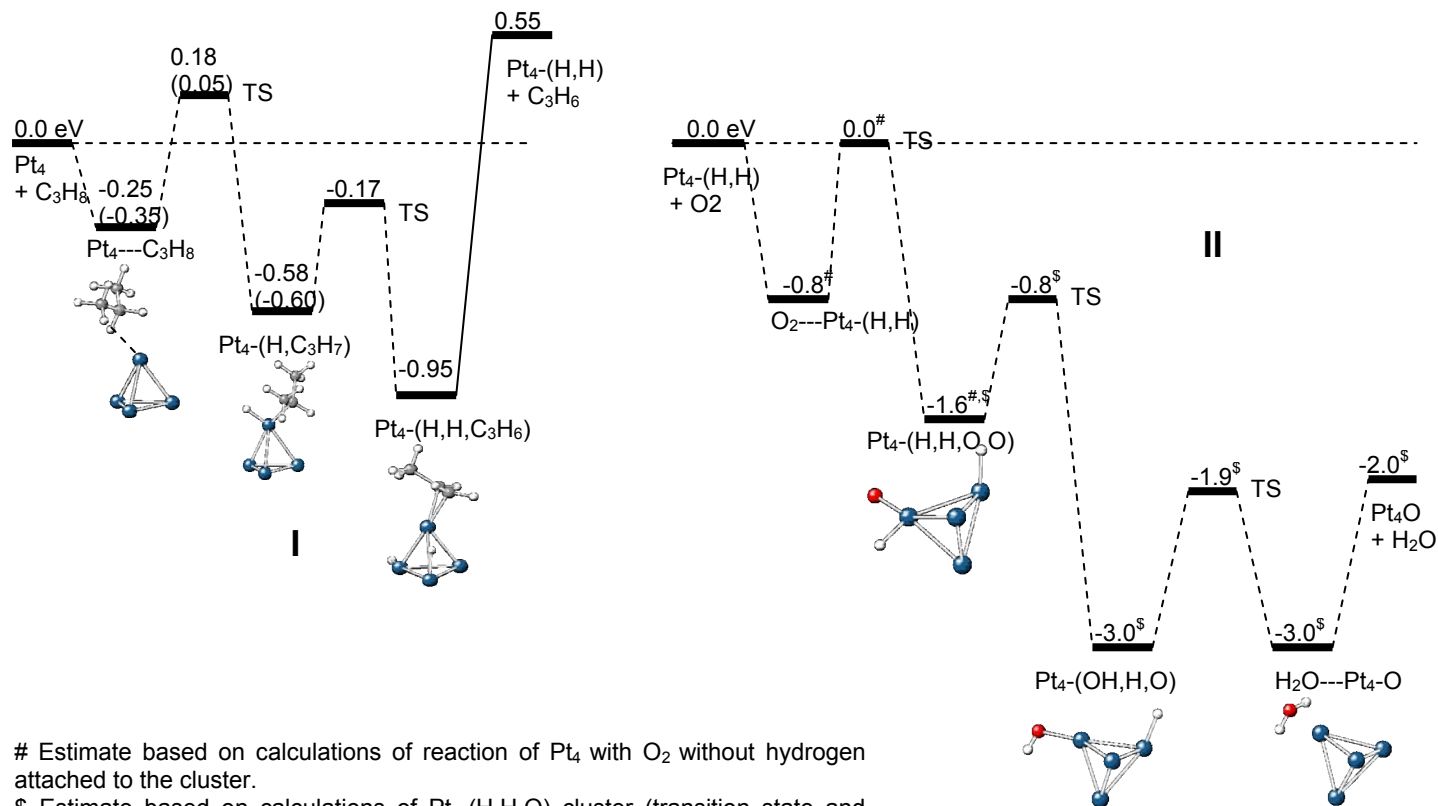
F1
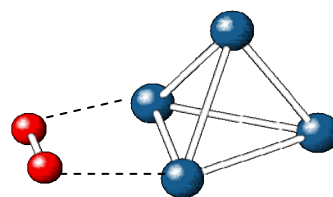
F2

F3

F4

Supplemental Figure 9. B3LYP structures for energies in Supplemental Table 8.

Supplemental Figure 10. B3LYP structures for energies in Supplemental Table 9.

Estimate based on calculations of reaction of Pt$_4$ with O$_2$ without hydrogen attached to the cluster.

$ Estimate based on calculations of Pt$_4$-(H,H,O) cluster (transition state and equilibrium structures). The effect of higher oxygen coverage is not considered, i.e. the second oxygen is not included in the calculation.

Supplemental Figure 11. Selected points on B3LYP potential energy surfaces: (I) reaction of propane with Pt$_4$ cluster; (II) reaction of O$_2$ with Pt$_4$-(H,H) cluster. Some of the energies shown are estimated values as described in the in the footnotes. Barriers for hydrogen transfer from Pt to Pt are not shown as they are smaller than those of hydrogen transfer from C to Pt or from Pt to H. Values in parentheses are calculated values for Pt$_8$ clusters. These results indicate that it is energetically favorable for hydrogen to react with dissociated oxygen on the Pt cluster to form water. This provides a mechanism for hydrogen removal in the overall reaction scheme.
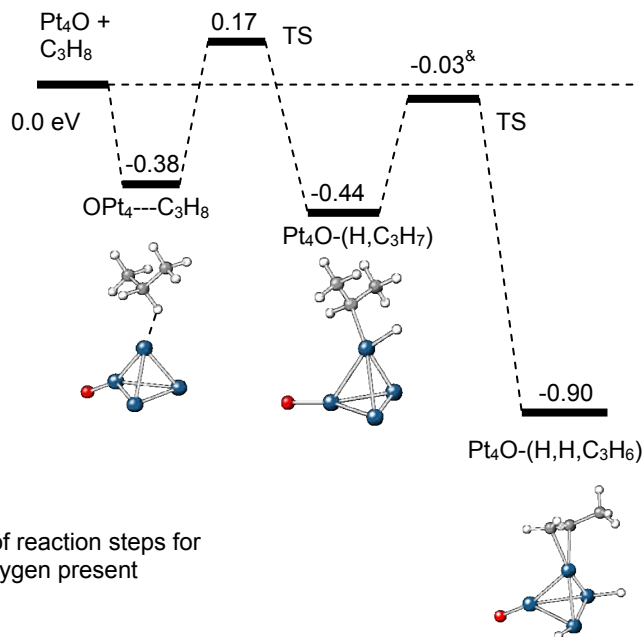
Supplemental Figure 12. Selected points on B3LYP potential energy surface of the reaction of propane with a Pt$_4$O cluster. These results show that dissociated oxygen on the cluster has little effect on the reaction pathway for C-H dissociation.